Lamellar Gels and Spontaneous Vesicles in Catanionic Surfactant Mixtures

Bret A. Coldren, Heidi Warriner, Ryan van Zanten, and Joseph A. Zasadzinski*

Department of Chemical Engineering, University of California, Santa Barbara, California 93106-5080

Eric B. Sirota

Exxon Research and Engineering Company, Corporate Strategic Research, Route 22 East, Annandale, New Jersey 08801

Caillé analysis of the small-angle X-ray line shape of the lamellar phase of 7:3 wt/wt cetyltrimethylammonium tosylate (CTAT)/sodium dodecylbenzene sulfonate (SDBS) bilayers shows that the bending elastic constant is $\kappa = (0.62 \pm 0.09)k_BT$. From this and previous results, the Gaussian curvature constant is $\bar{\kappa} = (-0.9 \pm 0.2)k_BT$. For 13:7 wt/wt CTAT/SDBS bilayers, the measured bending elasticity decreases with increasing water dilution, in good agreement with predictions based on renormalization theory, giving $\kappa_o = 0.28k_BT$. These results show that surfactant mixing is sufficient to make $\kappa \approx k_BT$, which promotes strong, Helfrich-type repulsion between bilayers that can dominate the van der Waals attraction. These are necessary conditions for spontaneous vesicles to be equilibrium structures. The measurements of the bending elasticity are confirmed by the transition of the lamellar phase of CTAT/SDBS from a turbid, viscoelastic gel to a translucent fluid as the water fraction is *decreased* below 40 wt %. Freeze-fracture electron microscopy shows that the gel is characterized by spherulite defects made possible by spontaneous bilayer curvature and low bending elasticity. This lamellar gel phase is common to a number of catanionic surfactant mixtures, suggesting that low bending elasticity and spontaneous curvature are typical of these mixtures that form spontaneous vesicles.

An open question is whether any unilamellar vesicles or, more specifically, spontaneous vesicles formed from cationic−anionic (also called catanionic) surfactant mixtures are at thermodynamic equilibrium or are simply a metastable organization on their way toward multilamellar liposomes (or, more properly, lamellar-phase dispersions in excess water).[1−7] Lamellar-phase liposomes are characterized by a well-defined bilayer spacing suggesting a balance between attractive and repulsive bilayer interactions that can overcome the translational entropic penalty of forming independent vesicles. Hence, in order for unilamellar vesicles to be stable relative to a multilamellar phase in excess water, bilayer interactions must be repulsive to neutral so that the system does not prefer multilamellar stacking. There are at least three distinct ways that unilamellar vesicle phases can be stabilized with respect to multilamellar phases discussed in the current literature.[1,4,8,9]

The first way to stabilize vesicles is for the surfactant bilayer to develop spontaneous curvature.[1,10−12] According to the original development of liquid crystal elasticity theory by Frank,[13] spontaneous curvature occurs only if there is an asymmetry between the sides of a smectic layer. In mixed anionic and cationic bilayers, this can occur because of a corresponding asymmetry in the composition of the inner and outer monolayers.[5,11,12] Vesicles whose radii are similar to the spontaneous curvature radius minimize the curvature energy relative to that of the corresponding flat lamellae. If the bending elasticity of the membrane is sufficiently large, then variations from the spontaneous curvature radius are sufficiently unfavorable that multilamellar vesicles are prohibited, even in the presence of weakly to moderately attractive bilayer interactions, especially at low concentrations where the translational entropy favors unilamellar vesicles.[5,11,12] Hence, a monodisperse population of spontaneously formed, unilamellar vesicles implies that stabilization results from spontaneous curvature and a large bending constant.[1,2,14] At higher concentrations or in the presence of stronger attractive bilayer interactions, this mechanism can lead to stable vesicles with a discrete but small number of bilayers because the interaction energy can overcome the increase in curvature energy for a limited deviation away from spontaneous curvature.[1] At sufficiently high concentrations, however, steric constraints lead to the coexistence of vesicles with a multilamellar phase.[10,12]

In the second mechanism, a stable multilamellar liposome phase is prevented at low concentrations by the increased translational entropy of many small unilamellar vesicles relative to a multilamellar phase in combination with a long-range repulsive interactions between the bilayers.[4,15,16] Electrostatic interactions can stabilize vesicles against aggregation at suf-

* To whom correspondence should be addressed. E-mail: gorilla@engineering.ucsb.edu. Phone: 805-893-4768. Fax: 805-893-4731.

(1) Jung, H. T.; Coldren, B.; Zasadzinski, J. A.; Iampietro, D. J.; Kaler, E. W. *Proc. Natl. Acad. Sci. U.S.A.* **2001**, *98*, 1353−1357.

(2) Jung, H. T.; Lee, Y. S.; Kaler, E. W.; Coldren, B.; Zasadzinski, J. A. *Proc. Natl. Acad. Sci. U.S.A.* **2002**, *99*, 15318−15322.

(3) Xia, Y.; Goldmints, I.; Johnson, P. W.; Hatton, T. A.; Bose, A. *Langmuir* **2002**, *18*, 3822−3828.

(4) Dubois, M.; Deme, B.; Gulik-Krzywicki, T.; Dedieu, J. C.; Vautrin, C.; Desert, S.; Perez, E.; Zemb, T. *Nature* **2001**, *411*, 672−675.

(5) Safran, S. A. *Surf. Sci.* **2002**, *500*, 127−146.

(6) Gradzielski, M. *J. Phys.: Condens. Matter* **2003**, *15*, R655−R697.

(7) Almgren, M.; Rangelov, S. *Langmuir* **2004**, *20*, 6611−6618.

(8) Rovira-Bru, M.; Thompson, D. H.; Szleifer, I. *Biophys. J.* **2002**, *83*, 2419−2439.

(9) Kaler, E. W.; Herrington, K. L.; Iampietro, D. J.; Coldren, B.; Jung, H. T.; Zasadzinski, J. A. Phase Behavior and Microstructure in Aqueous Mixtures of Cationic and Anionic Surfactants. In *Mixed Surfactant Systems*, 2nd ed.; Abe, M., Scamehorn, J., Eds.; Marcel Dekker: New York, 2005; pp 298−338.

(10) Kaler, E. W.; Murthy, A. K.; Rodriguez, B. E.; Zasadzinski, J. A. N. *Science* **1989**, *245*, 1371−1374.

(11) Safran, S. A., Pincus, P. A., Andelman, D. *Science* **1990**, *248*, 354−356.

(12) Safran, S. A.; Pincus, P. A.; Andelman, D.; MacKintosh, F. C. *Phys. Rev. A* **1991**, *43*, 1071−1078.

(13) Frank, F. C. *Discuss. Faraday Soc.* **1958**, *25*, 19−28.

(14) Coldren, B. A.; van Zanten, R.; Mackel, M. J.; Zasadzinski, J. A.; Jung, H. T. *Langmuir* **2003**, *19*, 5632−5639.

ficiently low salt and surfactant concentrations.[4,15,16] The best example of this mechanism is the large, polyhedral vesicles found in mixtures of fatty acids and hyroxide surfactants,[4] whose counterions combine to form water.[4,15,16] As a result, the background electrolyte concentration remains small ($\sim 10^{-7}$ M), and electrostatic interactions between the bilayers are large. These vesicles are stable only at relatively low surfactant concentrations in the absence of any added salt. Sufficient repulsive interactions between bilayers may also be generated by adding polymer—lipids such as polyethylene—glycol dipalmitoylphosphatidyle-thanolamine (PEG—DPPE); PEG—DPPE can stabilize vesicles by steric interactions and lead to unilamellar vesicles at low surfactant concentrations.[8]

Even in the absence of electrostatic interactions and in the high-salt environments common to mixtures of anionic and cationic surfactants, vesicles can be stabilized by the gain in entropy resulting from the large number of finite-sized vesicles.[10] This will always be the case at sufficiently low surfactant concentration, although in practice the concentration may need to be vanishingly small to stabilize vesicles.[5,17] However, if the bending elastic constant, $\kappa \approx k_B T$, then the repulsive Helfrich undulation interaction, which is inversely proportional to the bending elastic constant,[5,18] can overcome the attractive van der Waals interactions between the bilayers. The smaller the bending constant, the larger the repulsive interactions between layers; the net interaction between bilayers can be repulsive, and multila-mellar vesicles are prohibited in excess water.[1] A small elastic constant can favor vesicles even in the absence of spontaneous curvature essentially up to the close packing of vesicles, where at sufficiently high concentrations packing constraints lead to the coexistence of vesicles with a multilamellar phase.[9]

Bilayer Bending Elasticity and Thermodynamic Stability. Hence, to ascertain if vesicles can be thermodynamically stable relative to a multilamellar phase in excess water requires knowing at least the order of magnitude of the bilayer bending elasticity. The starting point for the description of bilayer elasticity in solution is the harmonic approximation to the bending free energy:

$$F_B = \int dA \left[\frac{1}{2}\kappa \left(\frac{1}{R_1} + \frac{1}{R_2} - \frac{2}{R_0} \right)^2 + \bar{\kappa} \left(\frac{1}{R_1 R_2} \right) \right] \quad (1)$$

Equation 1 was derived from the limiting case for thermotropic smectic phases[13] by Helfrich over 30 years ago and is universally used to describe monolayer and bilayer deformations at constant bilayer spacing or for the isolated bilayers in unilamellar vesicles.[5,19] R_1 and R_2 are the principle radii of curvature (for spherical vesicles, $R_1 = R_2 = R$, the vesicle radius), R_0 is the spontaneous radius of curvature, κ and $\bar{\kappa}$ are the mean and Gaussian bending constants, respectively, and A is the area of the bilayer. The harmonic approximation is appropriate when the bilayer thickness ($\sim 3-4$ nm) and the Debye length[17] for ionic surfactants are small compared to R_1 and R_2. However, the two elastic constants, κ and $\bar{\kappa}$, play very different roles in determining the bilayer organization.

The magnitude of κ determines the energy needed to bend the bilayer away from its spontaneous radius of curvature, R_0. For single-component or otherwise symmetric bilayers, $1/R_0 = 0$ by

symmetry;[5,12,13,18] a nonzero bilayer curvature is possible only when nonideal surfactant mixing causes the interior and exterior monolayers of the bilayer to have different compositions or environments.[5,12] However, $\bar{\kappa}$ influences only the topology (and hence the number) of the structures formed.[2] The Gauss—Bonnet theorem states that the integral of the Gaussian curvature over a given surface depends only on the genus of the structure.[20] Hence, the magnitude of $\bar{\kappa}$ has little effect at equilibrium as long as structural fluctuations take place at constant topology (as in a multilamellar phase) or vesicle number. However, the distribu-tion of surfactant between vesicles depends on the sum of $\kappa + (\bar{\kappa}/2)$.[1]

Although eq 1 has become the accepted description of the energetics of bilayer organization, there are relatively few measurements of κ and almost no measurements of $\bar{\kappa}$ for surfactant or lipid bilayer structures. There is also little explicit evidence to support the existence of bilayer spontaneous curvature.[1,2] Moreover, there are no generally accepted methods for deter-mining these elastic constants. $\bar{\kappa}$ is especially difficult to measure because it influences topological transformations between structures such as disks, spheres, and toroids,[2] or the distribution of material between vesicles,[1,5,12] or the transition between lamellar and L_3 phases. However, $\bar{\kappa}$ does not influence the more readily measured fluctuations of an equilibrium structure, and it has little influence on membrane interactions.

A key requirement to the understanding and possible control of surfactant structural organization is developing both experi-mental and theoretical tools to relate R_0, κ, and $\bar{\kappa}$ to surfactant molecular structure and solution conditions. Values of R_0 and the sum $\kappa + (\bar{\kappa}/2)$ for different cationic and anionic surfactant mixtures have been determined from the size distributions of the spontaneous vesicle phases of catanionic surfactant mixtures.[1,2,9,14] For all mixtures of hydrogenated surfactants studied, $\kappa + (\bar{\kappa}/2)$ was on the order of $k_B T$.[1,2,9,14] However, the individual constants, κ and $\bar{\kappa}$, could not be determined independently from the size distributions. Because $\bar{\kappa}$ can be either positive or negative (stability requires $\kappa > 0$ [19]), $\kappa + (\bar{\kappa}/2)$ can remain small as observed for the cationic—anionic vesicles if both κ and $\bar{\kappa}$ increase in magnitude but with opposite signs.[2] What really is necessary is another method of measuring either κ or $\bar{\kappa}$ independently so that the variation in the individual parameters with molecular structure can be ascertained. Although Brocca et al.[21] have measured the shape fluctuations of $\sim$100-nm-diameter phospholipid vesicles by light scattering, they have not been able to relate the observed fluctuations directly to a value of κ.

One method that has been used to extract κ is the analysis of bilayer fluctuations of lamellar phases at higher surfactant concentration. Safinya and co-workers have shown that the bending modulus, κ, can be determined from an analysis of the small-angle synchrotron X-ray scattering from the lamellar phase.[22-25] To evaluate κ quantitatively, Caillé line shape analysis of the small-angle X-ray scattering from the lamellar phase was performed,[22,23,25-27] confirming that $\kappa \approx k_B T$ for two different CTAT/SDBS ratios. From this analysis, surfactant mixing is

(15) Dubois, M.; Gulik-Krzywicki, T.; Deme, B.; Zemb, T. *C. R. Acad. Sci., Ser. IIc: Chim.* **1998**, *9*, 567−575.

(16) Dubois, M.; Lizunov, V.; Meister, A.; Gulik-Krzywicki, T.; Verbavatz, J. M.; Perez, E.; Zimmerberg, J.; Zemb, T. *Proc. Natl. Acad. Sci. U.S.A.* **2004**, *101*, 15082−15087.

(17) Israelachvili, J. N. *Intermolecular and Surface Forces*, 2nd ed.; Academic Press: London, 1992.

(18) Helfrich, W. *Z. Naturforsc.* **1978**, *33A*, 305−315.

(19) Helfrich, W. *Z. Naturforsch.* **1973**, *28C*, 693−703.

(20) Hilbert, D.; Cohn-Vossen, S. *Geometry and the Imagination*; Chelsea: New York, 1983.

(21) Brocca, P.; Cantu, L.; Corti, M.; Del Favero, E.; Motta, S. *Langmuir* **2004**, *20*, 2141−2148.

(22) Safinya, C.; Roux, D.; Smith, G. S.; Sinha, S. K.; Dimon, P.; Clark, N.; Bellocq, A. M. *Phys. Rev. Lett.* **1986**, *57*, 2718−2721.

(23) Safinya, C. R.; Sirota, E. B.; Roux, D.; Smith, G. S. *Phys. Rev. Lett.* **1989**, *62*, 1134−1137.

(24) Warriner, H.; Idziak, S.; Slack, N.; Davidson, P.; Safinya, C. *Science* **1996**, *271*, 969−973.

(25) Warriner, H. E.; Keller, S. L.; Idziak, S. H. J.; Slack, N. L.; Davidson, P.; Zasadzinski, J. A.; Safinya, C. R. *Biophys. J.* **1998**, *75*, 272−293.

(26) Roux, D.; Safinya, C. R. *J. Phys. (Orsay, Fr.)* **1988**, *49*, 307−318.

sufficient to provide the low values of the bending elasticity necessary to stabilize a spontaneous vesicle phase. From previous cryo-TEM measurements of the vesicle size distributions,[14,27] $\kappa + (\bar{\kappa}/2)$ has been determined for chemically similar systems so that we can show that $\bar{\kappa}$ is also $\sim k_B T$ but negative. Hence, it appears that (1) catanionic vesicles are thermodynamically stabilized by entropy; (2) there is spontaneous bilayer curvature; and (3) multilamellar liposomes are inhibited from forming by the Helfrich undulation interaction. Although this does not guarantee that spontaneous vesicles are at thermodynamic equilibrium, these are the necessary ingredients for thermodynamic stability.

These low values of the elastic constants also have interesting implications for the lamellar phase. For water fractions between 50 and 75%, a lamellar gel forms from CTAT/SDBS mixtures that freeze-fracture transmission electron microscopy (TEM) reveals has spherulite texture with a large number of defects, similar to lamellar gels of dimyristoylphosphatidylcholine, pentanol, and poly(ethylene glycol)−lipids.[24,25,28] At 40% water volume fraction, the lamellar phase becomes fluid and translucent; freeze-fracture TEM shows that the bilayers are flat and well-aligned. A simple defect-based theory of this structural progression requires that $\kappa \approx k_B T$ and that bilayer spontaneous curvature exists, confirming the small-angle scattering and cryo-TEM results.[24,25,28] We have found similar lamellar gel phases in equilibrium with other catanionic spontaneous vesicle systems,[27] suggesting that a small bending modulus and spontaneous curvature are common to many of these catanionic mixtures. Surprisingly, adding pentanol to the lamellar gel phase eliminates the defects in the bilayers, and the lamellar phase becomes fluid at all water fractions. The pentanol, which usually lowers the bending modulus,[24,25] causes the spontaneous curvature radius to increase, likely by diluting the concentration difference between the inside and outside monolayers of the bilayer. The increase in the spontaneous curvature radius causes the fluid lamellar phase to be stable to higher water dilutions.[24,25] This suggests that pentanol and other small molecules that partition equally well between the inside and outside monolayers of spontaneous vesicles might be used to tune the mean size of the vesicle distribution.

Materials and Methods

Materials. Cetyltrimethylammonium *p*-toluenesulfonate (CTAT, 98% pure, Sigma), dodecyltrimethylammonium chloride (DTAC, 98% pure, Fluka), and sodium dodecylbenzene sulfonate (SDBS, 99% pure, TCI America) were used as received. In all experiments, water was purified by the Milli-Q process, which results in a resistance of 18.2 MΩ. Brine solutions were prepared from mixtures of Milli-Q water and NaCl salts of >99.9% purity (Aldrich) to minimize the effect of electrostatics on the X-ray line shape. At these salt concentrations, the Debye screening length is <0.6 nm,[17] so electrostatic interactions are insignificant at lattice spacings greater than ∼3 nm.[22] In addition to the added salts, the cationic mixtures have significant concentrations of free counterions in solution so that the actual Debye length is substantially less than 0.6 nm. Samples were prepared by gentle mixing and heating cycles and were allowed to equilibrate for at least 2 months undisturbed before X-ray or freeze-fracture analysis.

Small-Angle X-ray Diffraction. Preliminary phase behavior and scattering experiments at UCSB were performed on two different custom-built instruments with 18 kW Rigaku rotating anode sources

(Cu Kα, $\lambda = 1.54$ Å) and 2-D area detectors. One instrument is set up for intermediate length scales (10−100 Å) and has a bent graphite monochromator, an 18 cm Mar image plate detector, and four sets of Huber slits. The 0.8×0.8 mm² beam has a flux of $\sim10^7$ photons/s. The fwhm was ~0.01 Å^{-1}. The second instrument is optimized for very small angle work (50−600 Å), has an Osmic Confocal Maxflux double-focusing multilayer mirror, an 11 cm Bruker HI-STAR multiwire area detector, and a 1.5 m sample-to-detector distance. The fwhm was less than ~0.005 Å^{-1}. In all experiments, samples were loaded into 1.5 mm borosilicate glass capillaries (Charles Supper, Natick, MA) and flame sealed. Temperature control was via circulating heated or cooled fluid through an aluminum sample holder block, monitored by a thermistor located adjacent to the capillary.

For Caillé line shape analysis of lamellar phases, the ExxonMobil X10A beamline at Brookhaven National Laboratory's National Synchrotron Light Source (NSLS) was used. A double-crystal (Ge-⟨111⟩) monochromator, narrow-slit geometry, and silicon crystal analyzer result in a typical in-plane resolution having a fwhm of just 0.0004 Å, corresponding to a resolution of ~3 μm. Scattering was detected using a Bicron point detector (Bicron, OH). After background subtraction, the SAXS peaks were fit to eq 7 using a numerical routine that minimize $\chi2$ as in Warriner et al.[25]

Freeze-Fracture Electron Microscopy. Freeze-fracture samples were prepared by first depositing a film of sample liquid approximately 100 micrometers thick between two copper planchettes. The samples were frozen by plunging the sample into a liquid propane/liquid ethane bath cooled by liquid nitrogen. The frozen sample was transferred under liquid nitrogen to the sample block of a JEM Cryofract freeze-fracture device. The block was then quickly transferred to the vacuum chamber of the Cryofract device via an airlock. After temperature (−170 °C) and pressure (<10−7 Torr) equilibration, the sample was fractured, and the two resulting surfaces were replicated with approximately 1.5 nm of platinum deposited at a 45° angle, followed by about 15 nm of carbon deposited normal to the surface. The replicas were then removed from the vacuum and warmed to room temperature. The copper planchettes were dissolved in chromerge (a mixture of chromic acid, sulfuric acid, and water), and then the replicas were washed in water and allowed to stand in ethanol several days to dissolve any remaining surfactant. The replicas were collected on Formvar-coated TEM grids (Ted Pella, Redding, CA).[29] A Gatan CCD camera was used to record digital bright-field images using a JEOL 100CXII TEM.

Rheological Measurements. The viscoelastic properties of the lamellar phases were quantitatively investigated using a Rheometric Ares controlled strain rheometer operated by Rheometric Scientific control software. Cone-and-plate geometry was employed with a 0.05 mm gap, 400 mm diameter, and 0.04 rad pitch. The ambient temperature was 25 ± 1 °C. A solvent-saturated (water) housing enclosed the sample in order to prevent evaporation. The lower plate is driven by a motor, in either steady rotation or oscillation, and the upper plate is connected to a transducer, which measures torque and normal force.

The samples were centrifuged free of bubbles, and an amount sufficient to fill the cone and plate gap completely was carefully scooped out and spread over the cone (∼1 mL). The upper plate was carefully lowered so as to avoid the formation of any bubbles in the gap. Samples were subjected to two standard oscillatory tests in order to determine G' and G'' as a function of frequency. First, a dynamic strain sweep test was performed (at a frequency of 10 rad/s) to determine the limits of the linear viscoelastic assumption. This is indicated by a range of strains for which the storage modulus, G', is invariant. For all measurements, a 1% strain was found to be optimal. Second, a dynamic frequency test is performed within the linear viscoelastic regime over a range of 0.01−100 rad/s to determine G' and G''. This test was performed from low to high frequency and vice versa to check for hysteresis. None was observed, so it was assumed that the sample microstructure was not being perturbed

(27) Coldren, B. Phase Behavior, Microstructure and Measured Elasticity of Catanionic Surfactant Bilayers. Ph.D. Dissertation, University of California, Santa Barbara, CA, 2002.

(28) Keller, S. L.; Warriner, H.; Safinya, C.; Zasadzinski, J. A. *Phys. Rev. Lett.* **1997**, *78*, 4781−4784.

(29) Zasadzinski, J. A.; Bailey, S. M. *J. Electron Microsc. Tech.* **1989**, *13*, 309−334.
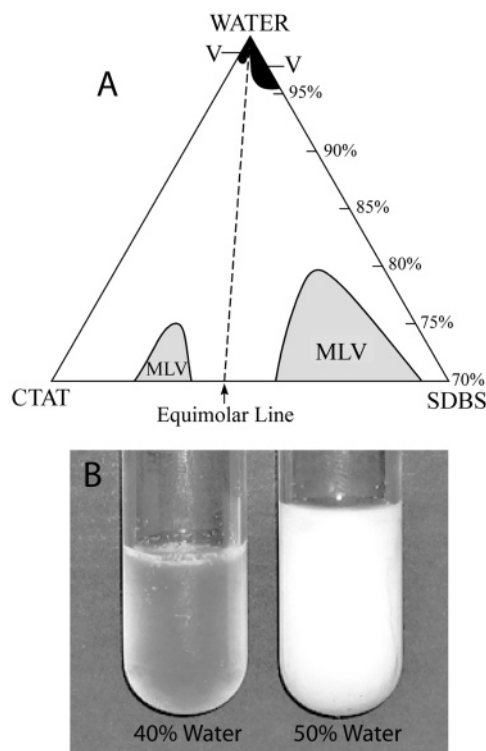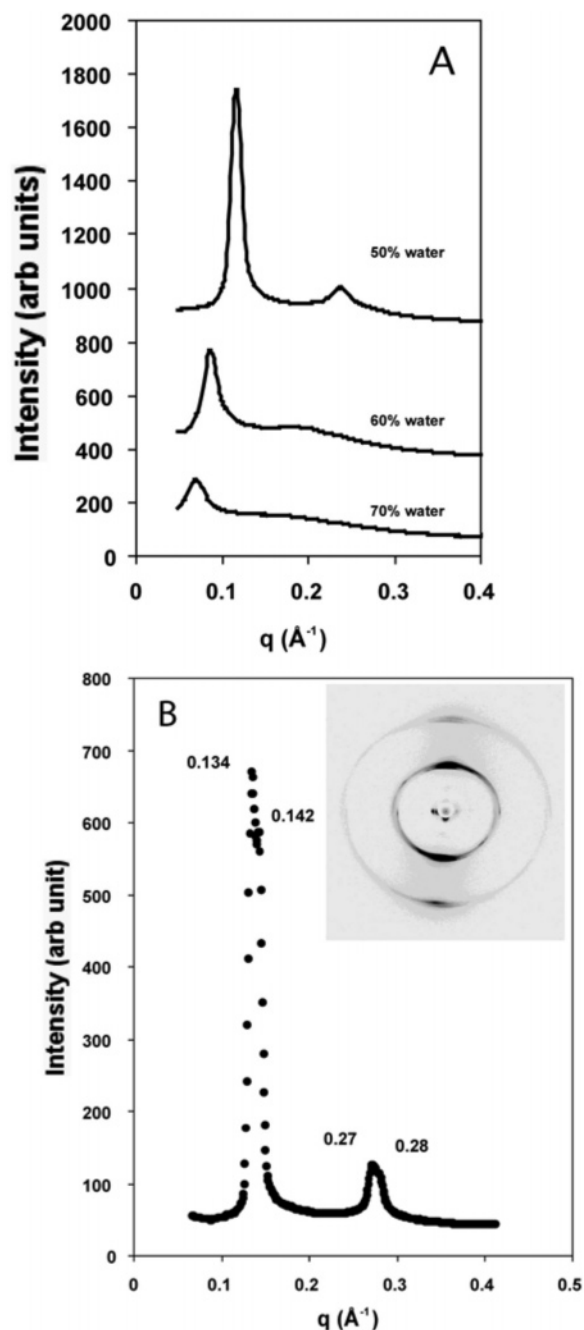
Figure 1. Partial phase diagram of CTAT/SDBS/water at 25 °C. MLV phases are onionlike multilamellar spherulites with no excess water that form a lamellar gel similar to DMPC/pentanol/polymer lipid gels.[24,25,28] V indicates stable unilamellar vesicles. Not indicated are micellar phases at either extreme of the surfactant mixing ratio. The MLV phase extends to ~50 wt % surfactant (not shown), where it transforms into a more fluid lamellar phase. CTAT/SDBS lamellar phases (7:3 wt/wt) in water at (left) 40% and (right) 50% water fractions. The 40% sample is clear and relatively fluid, and the 50% sample is opaque and exhibits a yield stress and a high viscosity.

(aligned) during the course of the rheological measurement. The third and final test was a nonoscillatory measurement of the steady complex viscosity as a function of strain rate. The complex viscosity was observed for 20 s at each strain rate over the range of 10^{-4} to 100 s^{-1}. Once again, no hysteresis was observed upon repeating the test.

Results and Discussion

Characterization of the Lamellar Phases of CTAT/SDBS. Dilute mixtures of CTAT/SDBS in aqueous solution were the first catanionic systems reported to form unilamellar vesicles spontaneously.[9,10] Cryo-TEM analysis of the size distribution of vesicles of 7:3 wt/wt CTAT/SDBS at 1% total surfactant in water showed that $\kappa + (\bar{\kappa}/2) = (0.15 \pm 0.03)k_\text{B}T$ and $R_0 = 55 \pm 10$ nm, suggesting that the vesicle phase was stabilized by entropy and the Helfrich undulation repulsion.[14,27] From the phase diagram (Figure 1), for surfactant concentrations >3 wt %, the vesicles become overcrowded, start to nest within each another, and grow in size.[30] Above 20−25% total surfactant, the entire sample volume is occupied by a lamellar liquid crystal or L_α phase. At intermediate concentrations, there is a continuous transition from dilute noninteracting vesicles to the L_α phase, as predicted theoretically.[31] The CTAT/SDBS system is nearly symmetric about the equimolar mixing ratio and presents two vesicle phases and two lamellar phases, one each of positive and negative net charge. The phase behavior in 0.25 M brine is similar for the

(30) Kaler, E. W.; Herrington, K. L.; Murthy, A. K.; Zasadzinski, J. A. N. *J. Phys. Chem.* **1992**, *96*, 6698−6707.
(31) Simons, B. D.; Cates, M. E. *J. Phys. II (Orsay, Fr.)* **1992**, *2*, 1439−1451.

Figure 2. Small-angle X-ray scattering (SAXS) spectra for 7:3 wt/wt CTAT/SDBS in water at 25 °C. (A) Primary peaks move to lower *q* values with increasing water fraction as given by the classic lamellar dilution law (Table 1). (B) At 40 wt % water, the bilayers arrange into large domains that partially orient in the 1.5 mm scattering tubes, as seen in the upper right 2-D detector image. We also see evidence of the formation of two lamellar phases of distinct repeat spacing, although resolution is insufficient to characterize the two phases fully. This is likely due to the vicinity of the transition from the fluid to the gel phase at this concentration (Figure 1).

CTAT-rich half of the phase diagram, whereas the SDBS-rich side collapses to a precipitate. Therefore, we concentration on the CTAT-rich phases here. Catanionic phase behavior is only weakly dependent upon temperature.[9]

Low-resolution SAXS scans are shown in Figure 2. The primary peak and higher harmonics occur in the characteristic lamellar 1:2 pattern in reciprocal space and follow the classic dilution law $\delta = d \times \Phi_\text{mem}$ (δ is the bilayer membrane thickness, *d* is the layer repeat spacing, and Φ_mem is the surfactant volume fraction).

Table 1. Measured Small Angle X-ray Spacings and Peak Widths for 7:3 wt/wt CTAT/SDBS at Different Bilayer Membrane Fractions, Φ_{mem}[a]

$1/\Phi_{mem}$	q peak (Å^{-1})	d (Å)	fwhm (Å^{-1})
1.67	0.142	44.2	n/a
2.00	0.118	53.2	0.014
2.50	0.089	70.6	0.02
3.33	0.071	88.5	0.022

[a] The full width at half maximum (fwhm) is inversely proportional to the size of the correlated bilayer domains and goes from resolution-limited at the lowest $1/\Phi_{mem}$ to rather small domains of $\sim$10−20 bilayers at the maximum $1/\Phi_{mem}$. The bilayer thickness, δ, is related to d and Φ_{mem} by $\delta = d \times \Phi_{mem}$. A linear fit to the data in Table 1 yields a membrane thickness of 27 ± 2 Å.

A linear fit to the data in Table 1 yields a membrane thickness of 27 ± 2 Å for 7:3 wt/wt CTAT/SDBS. The full width at half-maximum (fwhm) of the primary peaks scales inversely to the lamellar domain size; it is resolution-limited at 40% water but increases with $1/\Phi_{mem}$.

At 40% water, the reflections split into two peaks, suggesting the coexistence of two lamellar structures having slightly different d spacings (Figure 2b). This is unusual and is reminiscent of coexisting lamellar phases reported in symmetric double-tailed ammonium surfactants (DDAB) in water.[32] However, because of limited spectrometer resolution, both sets of peaks cannot be resolved. On the basis of the apparent position of the peaks, the d spacings differ by no more than $\sim$2.5 Å of the 44 Å lattice. For water fractions greater than 40%, the lamellar phases have an unusually high viscosity and turbidity, suggestive of sub-micrometer domain sizes (Figure 2c), whereas for lower water fractions the lamellar phase becomes much more fluid and transparent.[25]

Small-Angle X-ray Scattering and Caillé Line Shape Analysis. The thickness of CTAT/SDBS membranes at a 7:3 weight ratio is reported to be $\delta = 32 \pm 1$ Å by the surface forces method.[33] This may be considered to be an upper estimate relative to scattering methods that define the bilayer based upon electron density. From the data in Table 1, $\delta = 27 \pm 2$ Å using SAXS peak positions as a function of water dilution. In either case, basic elasticity theory predicts these membranes to be quite stiff with $\kappa \approx 10k_BT$, neglecting heterogeneous chain-mixing effects.[23] However, this is inconsistent with the analysis of the small-angle X-ray scattering, which shows how important surfactant mixing is to bilayer elasticity.

The Caillé structure factor, originally developed to describe diffraction from smectic A liquid crystals, has been used successfully to describe scattering from both electrostatic-[26] and undulation-stabilized lamellar systems.[22,23,25] The Caillé theory relates the X-ray line shape to the membrane spacing, d, the bulk compression modulus, B, and the smectic splay elastic modulus, K ($K \equiv \kappa/d$). The theory starts with the Landau−De Gennes expression for the free-energy density (F/V) of a smectic A liquid crystal:[22,23,25]

$$\frac{F}{V} = \frac{1}{2}\left\{ B\left(\frac{\partial u}{\partial z}\right)^2 + K\left(\frac{\partial^2 u}{\partial x^2} + \frac{\partial^2 u}{\partial y^2}\right)^2 \right\} \tag{2}$$

$u(\mathbf{r})$ is the layer displacement in the z direction normal to the layers. The first term describes variations in the membrane thickness, which are proportional to B; the second term describes variations in the membrane splay, which are proportional to the

splay elastic modulus, K (this term is equivalent to the first term in the Helfrich bending-energy expression in eq 1 with $K = \kappa/d$; terms involving $\bar{\kappa}$ do not alter the free energy of the bulk lamellar phase and hence do not appear in Caillé theory). In two-dimensionally ordered materials, thermally induced mean-square layer displacements diverge logarithmically with the domain size, L, destroying long-range order, which causes the conventional delta-function Bragg peaks in a crystal to be replaced by power law divergences.[34] For a powder sample, profiles of the bilayer ($00l$) reflections have the asymptotic form[22]

$$S(q) \approx |q - q_{00l}|^{\eta_l - 1}$$

$$\eta_l \equiv \frac{l^2 q_{00l}^2 k_B T}{8\pi\sqrt{BK}} \qquad \text{if } \eta_l < 1 \tag{3}$$

Thus, the shape of the ($00l$) scattering peaks is determined by the elastic properties of the bilayer as $\eta^2 \approx 1/KB$. To distinguish clearly between changes in intermembrane interactions (B) and membrane rigidity (K), a more formal analysis is used to fit the X-ray line shapes. The real-space Caillé correlation function is given by[35]

$$G(\mathbf{r}) \propto \left(\frac{1}{\rho}\right)^{2\eta_l} \exp\left(-2\gamma\eta_l - \eta_l E_l\left(\frac{\rho^2}{4\lambda z}\right)\right) \tag{4}$$

in which $\lambda \equiv \sqrt{K/B}$, γ is Euler's constant, and E_l is the exponential integral function.

In a single crystal of domain size L, the structure factor is the Fourier transform of $G(\mathbf{r})$ multiplied by a finite-size factor

$$S(0, 0, q_z) \propto \int\int\int G(\mathbf{r})\, e^{-\pi r^2/L^2}\, e^{-i(\mathbf{q} - \mathbf{q}_z)\cdot\mathbf{r}}\, d^3\mathbf{r} \tag{5}$$

For a powder sample, $S(0, 0, q)$ is averaged over all solid angles in reciprocal space:

$$S(q - q_{00l}) \equiv \int S(0, 0, q_z)\, d\Omega_q \propto$$
$$\int_{-\infty}^{\infty} dz \int_0^{\infty} G(z, \rho)\, e^{-\pi r^2/L^2}\, \frac{\sin(qr)}{qr}\, e^{-q_{00l}z}\, d\rho \tag{6}$$

For each harmonic peak order of l, there are five fitted parameters: η_l, λ, L, q_{00l}, and the peak intensity I_l. For a given sample, all harmonics should give the same values of λ and L, but η_l should scale as l^2. From these fits, κ and B are readily extracted:

$$\frac{\kappa}{d} \equiv \frac{q_o^2 \lambda}{8\pi\eta}k_B T$$

$$B = \frac{k_B T}{8\pi}\left(\frac{q_o^2}{\eta\lambda}\right) \tag{7}$$

Figure 3 shows the full Caillé power law line shape fit to the first two harmonics of SAXS scans of CTAT/SDBS in a 7:3 wt/wt ratio in 50 wt % 0.25 M NaCl brine. The horizontal axis is normalized by subtracting the peak position, **G**, from the scattering vector, **q**. The vertical intensity axis is normalized by the peak intensity, $I(G)$ as in Warriner et al.[25] The fitting parameters yield $\kappa = (0.62 \pm 0.09)k_B T$, $B = (65 \pm 10) \times 10^5$ erg/cm^3, and $L = 1225 \pm 98$ Å, and the fit captures the asymmetry of the peaks quite well. The low value of κ shows that mixing

(32) Dubois, M.; Zemb, T. *Langmuir* **1991**, *7*, 1352−1360.
(33) Chiruvolu, S.; Israelachvili, J.; Naranjo, E.; Xu, Z.; Kaler, E. W.; Zasadzinski, J. A. *Langmuir* **1995**, *11*, 4256−4266.
(34) Caille, A. *C. R. Hebd. Seances Acad. Sci., Ser. B* **1972**, *274*, 891−893.
(35) Als-Nielsen, J.; Litster, J. D.; Birgeneau, R. J.; Kaplan, M.; Safinya, C. *Phys. Rev. B* **1980**, *22*, 312−320.
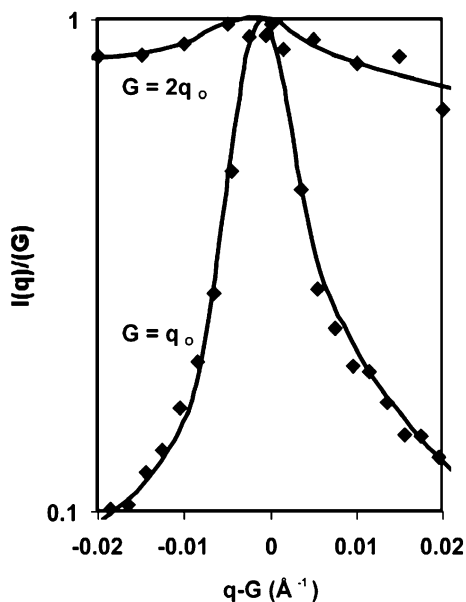
Figure 3. Fits of the full Caillé power law line shape to the two harmonics of SAXS scans of 7:3 wt/wt CTAT/SDBS in 50 wt % 0.25 M NaCl brine. The horizontal axis is normalized by subtracting the peak position, **G**, from the scattering vector, **q**. The vertical intensity axis is normalized by the peak intensity, $I(G)$. The fitting parameters yield $\kappa = (0.62 \pm 0.09)k_BT$, $B = (65 \pm 10) \times 10^5$ erg/cm^3, and $L = 1225 \pm 98$ Å.
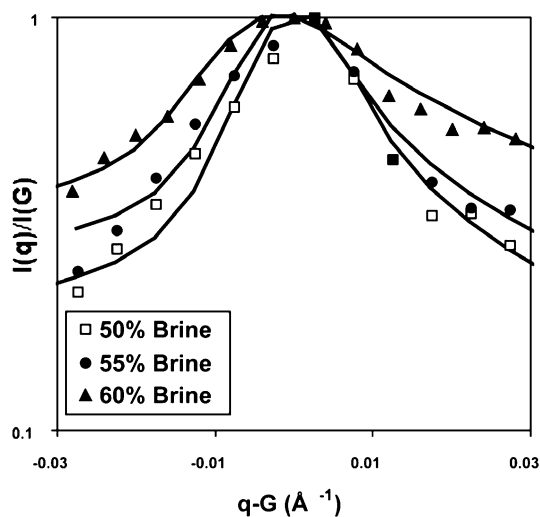
Figure 4. Fits of the full Caillé power law line shape to the first harmonics of SAXS scans of 13:7 wt/wt CTAT/SDBS at varying 0.25 M NaCl brine weight percentages. The horizontal axis is normalized by subtracting the peak position, **G**, from the scattering vector, **q**. The vertical intensity axis is normalized by the peak intensity, $I(G)$. For 50 wt % brine, the fitting parameters yield $\kappa = (0.23 \pm 0.04)k_BT$ and $L = 419 \pm 1$ Å. For 55 wt % brine, $\kappa = (0.16 \pm 0.04)k_BT$, and $L = 429 \pm 86$ Å. For 60 wt % brine, $\kappa = (0.06 \pm 0.01)k_BT$, and $L = 402 \pm 67$ Å. B decreases smoothly from $(70.7 \pm 13) \times 10^5$ to $(47.6 \pm 9) \times 10^5$ erg/cm^3 between 50 and 60% brine.

dramatically lowers the effective mean bending constant. From the cryo-TEM measured value of $\kappa + (\bar{\kappa}/2) = (0.15 \pm 0.03)k_BT$,[14] we calculate that $\bar{\kappa} = (-0.9 \pm 0.2)k_BT$. The negative value of $\bar{\kappa}$ promotes the formation of defects with positive curvature (consistent with the spherulite textures observed in the electron micrographs in Figure 5).

Figure 4 shows scattering profiles of the first harmonics of a series of three lamellar-phase samples at a slightly different CTAT/SDBS weight ratio of 13:7, which is also within the same multilamellar region of the phase diagram. The profiles are
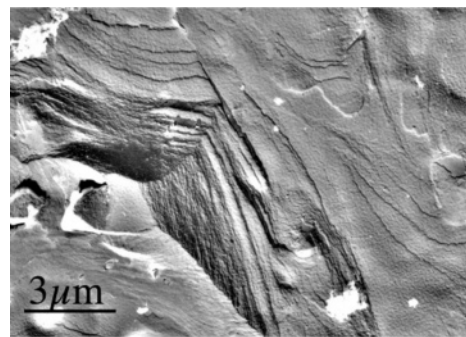
Figure 5. FF-TEM of a 7:3 wt/wt CTAT/SDBS, 40% water sample. Despite identical sample preparation and mixing as more dilute samples (Figures 6–8), a flat bilayer phase exists. Surprisingly, the viscosity of this high-membrane-volume-fraction sample is significantly less than that of the higher-dilution samples that show gellike behavior (Figure 7).

normalized to unit intensity, and the scattering vector is normalized by **q**−**G**, as in Figure 3. Again, the solid lines are fits of the full Caillé power law line shape. For 50 wt % brine, the fitting parameters yield a bending rigidity of $\kappa = (0.23 \pm 0.04)k_BT$ and a domain size of $L = 419 \pm 1$ Å. For 55 wt % brine, $\kappa = (0.16 \pm 0.04)k_BT$, and $L = 429 \pm 86$ Å. For 60 wt % brine, $\kappa = (0.06 \pm 0.01)k_BT$, and $L = 402 \pm 67$ Å. κ decreases with increasing brine volume fraction (or d), whereas L remains essentially constant. Helfrich[36] and others[37] have postulated that thermal fluctuations renormalize the effective elastic constants on the basis of the length scale of observation, here the lamellar d spacing, relative to δ, the bilayer thickness

$$\kappa = \kappa_o - \alpha \frac{k_BT}{4\pi} \ln\left(\frac{d - \delta}{\delta}\right) \qquad (8)$$

where the prefactor, α, is predicted to be 3, although this value is model-dependent.[37] Fitting the limited 13:7 data to eq 8 with $\delta = 2.7$ nm gives $\kappa_o = 0.28k_BT$ and $\alpha = 4.4$. The effect of thermal fluctuations, then, is to increase the apparent rigidity at small distances approaching the membrane thickness while decreasing the rigidity at large distances. However, it should be noted that this renormalization remains under scrutiny in the literature, and Helfrich has recently proposed that thermal fluctuations *stiffen* the membrane.[38] The compression modulus, B, decreases smoothly from 70.7 ± 13 to 47.6 ± 9 in units of 10^5 erg/cm^3 from 50 to 60% brine, which is consistent with the interbilayer repulsion being dominated by fluctuations.[18,23,25]

On the basis of the peak positions, the lamellar d spacings of the samples in Figure 4 vary between 5.9 and 7.7 nm, so the $L \approx 40$ nm domain size equates to 5–7 correlated bilayers in each domain. This high degree of disorder in the CTAT-rich lamellar-phase samples may raise concerns over the validity of the Caillé analysis (a potential source of the dramatically low measured κ). However, the line shapes fit the Caillé theory, and the fitted and calculated parameters have the expected scaling relationships. The low values of κ are also confirmed by the novel gel−fluid transition in the lamellar phase.

Gel-to-Fluid Lamellar Transition. Macroscopically, there is a profound difference between the translucent and fluid lamellar phase at 40% and the viscoelastic and opaque lamellar phase at 50% (Figure 1b). Surprisingly, increasing the water fraction increases the viscosity of the phase even though the d spacing of the lamellar phase increases as expected (Table 1). Figure 5

(36) Helfrich, W. *J. Phys. (Orsay, Fr.)* **1985**, *46*, 1263−1268.
(37) Peliti, L.; Leibler, S. *Phys. Rev. Lett.* **1985**, *54*, 1690−1693.
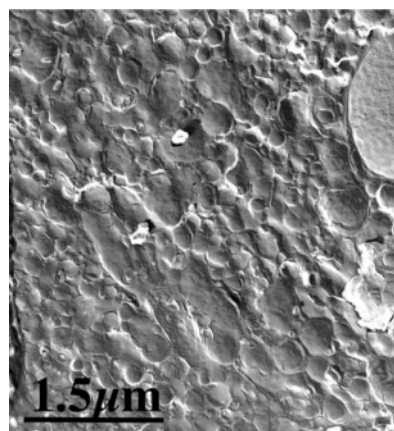(38) Pinnow, H. A.; Helfrich, W. *Eur. Phys. J. E* **2000**, *3*, 149−157.
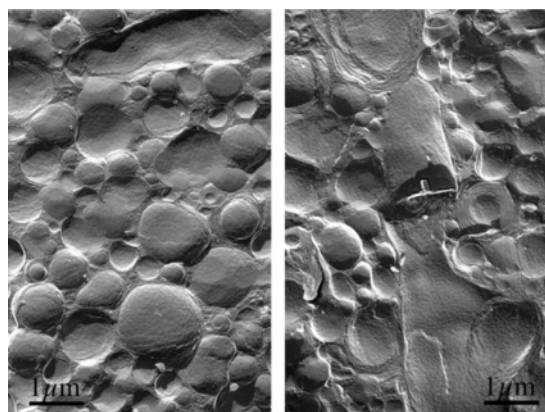
Figure 6. FF-TEM of a 7:3 wt/wt CTAT/SDBS, 50% water, single-phase sample near the multiphase boundary. Multilamellar spherulites are larger, on average about 1 micrometer, when compared to more dilute samples (Figures 7 and 8). Compare textures to the flat lamellar phase at 40% water in Figure 5 prepared in exactly the same way.
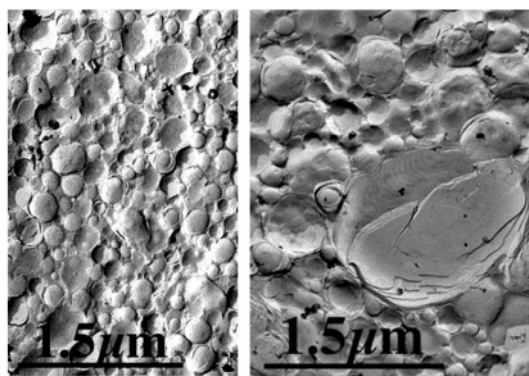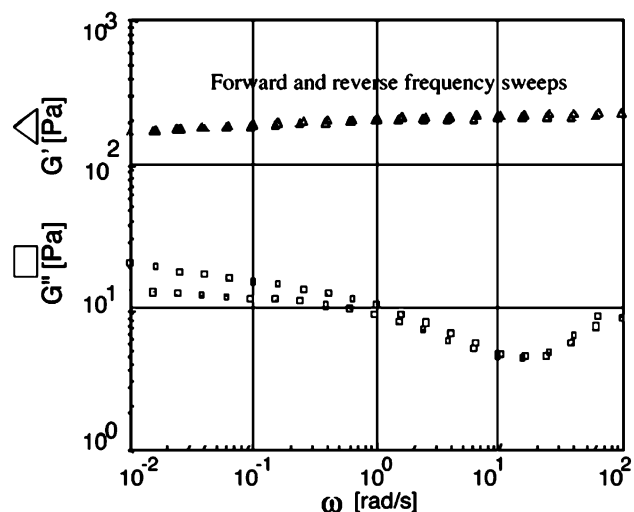

Figure 7. FF-TEM of a 7:3 wt/wt CTAT/SDBS, 70% water sample. The sample was prepared with mild stirring and heating, yet small but polydisperse multilamellar spherulites form spontaneously. Although the sizes of the spherulites range widely, the mean size is about 0.5 micrometers, about half that of the 50% water fraction sample (Figure 4).

shows a freeze-fracture TEM (FFTEM) image of 7:3 wt/wt CTAT/SDBS in 40% water. The image is typical of gently undulating but overall flat bilayers similar to other lipid and surfactant lamellar phases and thermotropic smectic phases.[25,29,39,40] The structure correlates well with the resolution-limited SAXS peaks, implying large lamellar domains (Figure 2). However, the FFTEM resolution of ~2 nm is too low to confirm coexisting lamellar phases having spacings that differ by only 0.2 nm.[41]

Freeze-fracture TEM (Figure 6) shows that at 50% water the lamellar organization is retained (consistent with the X-ray diffraction in Figure 2) but the domain size is greatly reduced and spherulite defect topology is present. These micrometer-sized domains correlate with a dramatic increase in turbidity and viscosity from 40 to 50% water. Increasing the water volume fraction to 70% (Figure 7) causes the domain size to decrease to 0.5 μm, consistent with the increases in the fwhm of the primary SAXS peak (Table 1). To confirm that the MLV topology is at equilibrium rather than due to sample preparation, a 7:3 wt/wt CTAT/SDBS with 70% water sample was heated to 100 °C (through an isotropic phase transition), followed by 1 year of
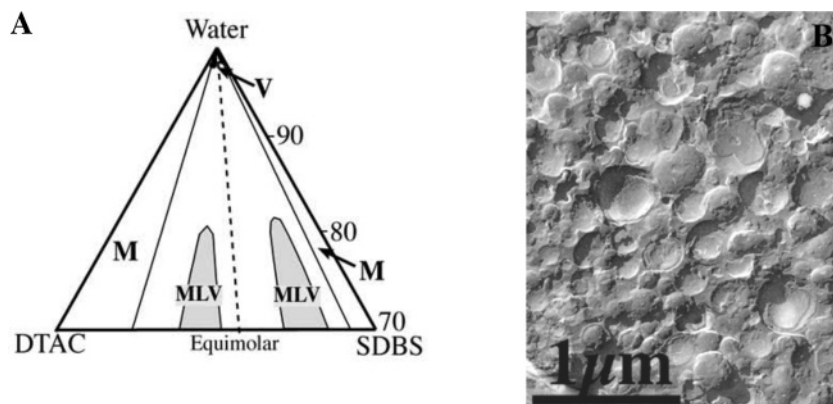
(39) Zasadzinski, J. A. *J. Phys.* **1990**, *51*, 747−756.
(40) Ihn, K. J.; Pindak, R.; Zasadzinski, J. A.; Slaney, A. J.; Goodby, J. *Science* **1992**, *258*, 275−278.
(41) Chiruvolu, S.; Naranjo, E.; Zasadzinski, J. A. *Microstructure of Complex Fluids by Electron Microscopy*; Herb, C. A., Prud'homme, R. K., Eds.; In ACS Symposium Series; American Chemical Society: Washington DC, 1994; Vol. 578, pp 86−104.

Figure 8. FF-TEM of a 7:3 wt/wt CTAT/SDBS. 70% water sample. The image was taken after annealing to 100 °C (transparent fluid), cooling, and 1 additional year at 25 °C. Spherulite "onion" membrane organization persists, suggesting that the spherulite texture is an equilibrium phenomenon. Compare to Figure 6, which shows the same distribution of spherulite sizes and shapes.

Figure 9. Dynamic frequency measurement of storage and loss moduli for a 7:3 wt/wt CTAT/SDBS, 70% water sample. Despite simple spherulite bilayer morphology, gellike properties are observed. Storage moduli, G', are 10-fold greater than viscous G'' moduli and nonvanishing in the limit of zero frequency, indicating a yield stress. Measurements made at 1% total strain and reverse frequency direction overlay well, indicating the lack of measurement hysteresis.

equilibration at 25 °C. Figure 8 shows that the spherulite topology is maintained and has a similar distribution of sizes to that of Figure 7.

This lamellar gel phase is similar structurally to the "onion" phases reported in numerous lamellar systems subjected to very strong shear flows[42] and to dilute, highly charged lamellar phases,[43] but this structure is found very rarely at equilibrium in dense lamellar phases. The very gentle mixing and heating that these CTAT/SDBS samples received cannot explain the spontaneous and stable formation of submicrometer structures, especially because the 40% water sample (Figure 5) shows flat, extended bilayers under the same mixing conditions. The spherulite defect structure in CTAT/SDBS is stable to added salt, unlike those reported by Hoffmann et al.[43]

Spherulite texture containing a large number of defects at high dilution progressing into flat layers at a lower water fraction

(42) Diat, O.; Roux, D. *J. Phys. II* **1993**, *3*, 9−14.
(43) Hoffmann, H.; Thunig, C.; Munkert, U.; Meyer, H. W.; Richter, W. *Faraday Discuss.* **1995**, *101*, 319−333.

Figure 10. (A) Phase diagram for DTAC/SDBS/water at 25°C. The MLV phase is turbid and viscoelastic, similar to that in the CTAT/SDBS/water system shown in Figure 1. M denotes micellar phases, and V denotes unilamellar vesicles. (B) Freeze-fracture TEM image of a 11:9 wt/wt DTAC/SDBS, 80% water sample showing similar spherulite defect textures to those in the CTAT/SDBS system.

has previously been found in lamellar gels formed from dimyristoylphosphatidylcholine, pentanol, and polymer−lipids but at much higher water fractions and d spacings.[24,25,28] To complete the analogy with the lamellar gels, dynamic frequency measurements of storage and loss moduli at 70% water composition are shown in Figure 9. The storage modulus, G', is 10-fold greater than the viscous loss moduli, G'', and is nonvanishing in the limit of zero frequency, indicating a yield stress of ∼100 Pa. The spherulite topology imparts gellike properties, as observed in the DMPC/pentanol/polymer−lipid system.[24,25,28]

This gel−fluid transition can be explained via a simple defect-based model that balances the curvature energy of bilayer defects with the defect entropy; the theory predicts that gelation requires a spontaneous bilayer curvature and $k \approx k_BT$. The relationship between the d spacing at the gel−fluid transition, d_{gel}, the spontaneous curvature radius, R_0, and κ is given by a balance between the curvature energy, E, and entropy, TS, of forming an edge dislocation pair of opposite Burgers vectors $2d_{gel}$.[24,25] The curvature energy per unit length of a straight-edge dislocation is (from eq 1, with $R_1 = d/2$ and $R_2 = \infty$)

$$\frac{E}{L} = \frac{\kappa}{2}\left(\frac{2}{d_{gel}} - \frac{2}{R_0}\right)^2 \pi d_{gel} \qquad (9)$$

(Curving the bilayers into spherulite defects will introduce additional terms into eq 9 that include the Gaussian curvature and likely lower the net energy of the defect.) The entropy per unit length, TS/L, of such a line defect is k_BT/ξ_p, in which ξ_p is the persistence length along the main axis of the defect:

$$\xi_p = \frac{\pi d_{gel}\kappa}{k_BT}$$

$$\frac{TS}{L} = \frac{(k_BT)^2}{\pi d_{gel}\kappa} \qquad (10)$$

These contributions balance at the gel point, which gives the following relation:[24,25]

$$d_{gel} \approx \frac{R_0}{2}\left(2 - \frac{\sqrt{2}k_BT}{\pi\kappa}\right) \qquad (11)$$

For the 7:3 CTAT/SDBS mixture, $d_{gel} = 5.3$ nm at 50% water; from the cryo-TEM analysis, $R_0 = 55$ nm,[14] which predicts $\kappa \approx 0.25k_BT$ (which is the same order of magnitude that we find from the X-ray line shape and is reasonable given the simplicity of

the model). The presence of the spherulite texture is confirmation of the cryo-TEM analysis of the spontaneous vesicle size distributions that invokes spontaneous curvature[1] as well the X-ray scattering that shows $\kappa \approx k_BT$. We find that most spontaneous vesicle phases stabilized by entropy and spontaneous curvature should have a turbid, gellike lamellar phase at a sufficiently high water fraction.[27]

As an example of the gel phase in a similar catanionic system, the phase diagram for dodecyltrimethylammonium chloride (DTAC) with SDBS is shown in Figure 10A; DTAC/SDBS also shows the gel lamellar phase (labeled MLV). DTAC has a shorter 12-carbon tail (compared to the 16 carbons in CTAT) and a fully dissociating chloride counterion (unlike CTAT's tosylate). Nevertheless, DTAC/SDBS mixtures have phase behavior similar to that of CTAT/SDBS. The MLV phase of DTAC/SDBS has the same high turbidity and viscosity of the lamellar gel phase of CTAT/SDBS. FF-TEM images (Figure 10B) of 11:9 wt/wt DTAC/SDBS shows the same spherulite defect morphology. The main difference is that DTAC/SDBS gel phases persist to slightly higher water dilutions. This is somewhat expected because a shorter hydrocarbon chain leads to thinner bilayers, which leads to a lower value of the bending rigidity, for which the thermal undulation repulsion is enhanced. Electrostatic repulsions may also be enhanced by increased dissociation of the DTAC counterion.

Effects of Pentanol on Spontaneous Curvature. Somewhat surprisingly, adding pentanol to the lamellar gel phase of CTAT/SDBS eliminates the gel phase and fluidizes the bilayers. Figure 11A shows the SAXS patterns of 7:3 wt/wt CTAT/SDBS with 50% NaCl brine as a function of the pentanol weight fraction. As the pentanol fraction is increased to 20 wt % (about 60% by mole fraction), a completely fluid lamellar phase is obtained, and the fwhm of the primary scattering peak becomes resolution-limited, suggesting larger, well-correlated lamellar domains. Further addition of pentanol solubilizes the bilayers into micelles. Figure 11B shows the same effect at 60 wt % brine; the lamellar gel becomes more fluidlike, and the X-ray peak is resolution-limited at 20 wt % brine.

Pentanol is often used in lipid bilayer studies to decrease κ.[22−25,28] However, for the CTAT/SDBS system, κ is already on the order of k_BT because of surfactant mixing, and eqs 9−11 predict that a decrease in κ should make bilayer defects lower in energy, leading to gel phases at lower water fractions and d spacings, the opposite of what is observed. A more likely explanation is that the added pentanol increases the spontaneous radius of curvature by diluting whatever concentration asymmetry exists in the CTAT/SDBS bilayer. Safran et al.[11] proposed that
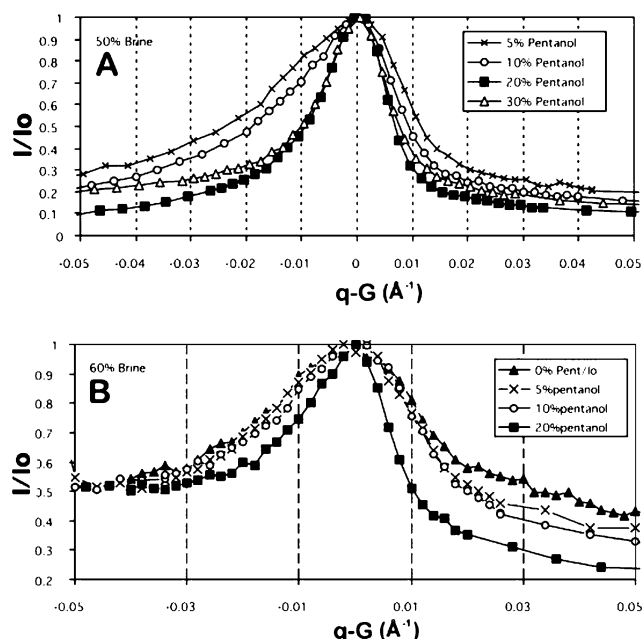
Figure 11. (A) Rescaled first-order scattering peaks of the lamellar phase of 7:3 wt/wt CTAT/SDBS with 50 wt % 0.25 M NaCl brine along the line of increasing pentanol weight fraction. The peak fwhm decreases dramatically for 20 wt % added pentanol, corresponding to the transition between the lamellar gel and fluid lamellar phases. Scans are resolution-limited at 20% pentanol; therefore, we cannot distinguish any further increase in domain size within the fluid lamellar phase. (B) Rescaled first-order scattering peaks of the lamellar phase of 7:3 wt/wt CTAT/SDBS in 60 wt % 0.25 M NaCl brine with increasing weight fractions of pentanol. Again, the dramatic decrease in fwhm corresponds to small onion domains reverting to a flat stacked lamellar phase when the bilayers contain 20 wt % pentanol.

the spontaneous curvature is the result of nonideal mixing leading to concentration differences between the different monolayers in the bilayer. However, in mixtures with lipids, adding pentanol does not lead to a spontaneous bilayer curvature, but rather pentanol appears to partition equally on both sides of the bilayer, leading to flat bilayers; the pentanol is capable of rapid equilibration across the bilayer.[25]

Hence, adding pentanol just dilutes whatever concentration asymmetry does exist in the bilayer. Alternately, for a given concentration asymmetry to exist with added pentanol, the radius of spontaneous curvature has to increase. The simplest model is that the spontaneous curvature should scale as $R_0/(1 -$ mole fraction of pentanol in the bilayer). Hence, 20 wt % pentanol is about 60 mol %, so R_0 should increase from about 55 to about 140 nm. If κ stays the same, then d_{gel} should increase from 5.3 to about 13.5 nm, which is significantly larger than the d

spacings of the lamellar phase even at maximum dilution (Table 1). Hence, the gel phase is unstable relative to the fluid phase, as is observed.

Conclusions

The existence of a lamellar gel at high dilutions that transforms into a fluid lamellar phase at lower dilutions confirms that CTAT/SDBS bilayers have a low bending elasticity, $\kappa \approx k_BT$, and a nonzero spontaneous curvature radius.[24,25,28] Caillé analysis of the small-angle X-ray line shape confirms that for 7:3 wt/wt CTAT/SDBS bilayers $\kappa = (0.62 \pm 0.09)k_BT$. From this and previous results, $\bar{\kappa} = (-0.9 \pm 0.2)k_BT$. For 13:7 wt/wt CTAT/SDBS bilayers, the measured bending elasticity decreases with increasing water dilution, in good agreement with predictions based on renormalization theory, giving $\kappa_o = 0.28k_BT$. These results show that surfactant mixing is sufficient to reduce the effective κ sufficiently to allow the formation of bilayers with strong, repulsive, Helfrich undulations that dominate the van der Waals attraction. Putting in some relevant numbers, for κ between $0.1k_BT$ and $0.6k_BT$, the Helfrich repulsion scales as $(0.3-2)$-k_BT/d_w^2, where $d_w = d - \delta$ is the spacing between adjacent membranes. With a Hamaker constant of about $(1-10)k_BT$, the unretarded van der Waals attraction scales as $E_{vdW} = (-0.03$ to $-0.3)k_BT/d_w^2$. Hence, the bilayer interactions should be repulsive at all separations, leading not only to the large lamellar dilutions observed in the phase diagrams for catanionic lamellar phases (Figures 1 and 10) but also to the thermal stabilization of spontaneous unilamellar vesicles. The combination of a nonzero spontaneous radius of curvature, small, positive κ, and small, negative $\bar{\kappa}$ explains both the existence of polydisperse, equilibrium unilamellar vesicles at high water fractions[1,2,14] and the lamellar gel-to-fluid phase transition at lower water fractions.[24,25] Hence, it appears that catanionic vesicles can be thermodynamically stabilized by entropy, that there is spontaneous bilayer curvature, and that multilamellar liposomes are inhibited from forming by the Helfrich undulation interaction. Although this does not guarantee that spontaneous vesicles are at thermodynamic equilibrium, these are the necessary ingredients for the thermodynamic stability of polydisperse, unilamellar catanionic vesicles and a fluid-to-gel lamellar transition.